Detecting hierarchical stellar systems with LISA

Travis Robson and Neil J. Cornish
eXtreme Gravity Institute, Department of Physics, Montana State University, Bozeman, Montana 59717, USA

Nicola Tamanini
Max-Planck-Institut für Gravitationsphysik, Albert-Einstein-Institut, Am Mühlenberg 1, 14476 Potsdam-Golm, Germany

Silvia Toonen
Anton Pannekoek Institute for Astronomy, University of Amsterdam, NL-1090 GE Amsterdam, Netherlands

(Received 1 June 2018; revised manuscript received 15 August 2018; published 10 September 2018)

A significant fraction of stars are members of gravitationally bound hierarchies containing three or more components. Almost all low-mass stars in binaries with periods shorter than three days are part of a hierarchical system. We therefore anticipate that a large fraction of compact galactic binaries detected by the Laser Interferometer Space Antenna will be members of hierarchical triple or quadruple system. The acceleration imparted by the hierarchical companions can be detected in the gravitational wave signal for outer periods as large as 100 years. For systems with periods that are shorter than, or comparable to, the mission lifetime, it will be possible to measure the period and eccentricity of the outer orbit. Laser Interferometer Space Antenna observations of hierarchical stellar systems will provide insight into stellar evolution, including the role that Lidov-Kozai oscillations play in driving systems toward merger.

DOI: 10.1103/PhysRevD.98.064012

I. INTRODUCTION

The Laser Interferometer Space Antenna (LISA) [1] is expected to individually resolve the signals from tens of thousands of compact galactic binaries during its nominal four year mission lifetime [2]. Roughly 13% of low-mass stellar systems contain three or more stars [3–5], and roughly 96% of low-mass binaries with periods shorter than 3 days are part of a larger hierarchy [6,7]. While the multiplicity distribution for ultracompact binaries is currently unknown, it is reasonable to expect that a significant fraction of compact galactic binary systems detected by LISA will be members of a hierarchical system. Indeed, dynamical effects in hierarchical stellar systems such as oscillations in the eccentricity due to the (regular eccentric) Lidov-Kozai mechanism [8–10] can cause the inner binary orbit to harden, potentially enhancing the fraction of compact binary systems with companions [11–17].

The hierarchal companions to the ultracompact binaries detected by LISA will impart accelerations on the center of mass of the binary that can lead to observable doppler shifts in the signals. This effect has previously been considered in the context of LISA observations of extreme mass ratio binaries [18] and merging black hole binaries detected by laser interferometer gravitational-wave observatory and LISA [19–22]. The mathematical description is essentially identical to that in pulsar timing, where the orbital parameters of pulsars found in binary systems can be inferred from modulations of the radio pulses [23]. One difference between the radio and gravitational wave analyses is that wavelengths of the gravitational waves are significantly larger than the gravitational radii of the stars, which modifies the calculation of the Shapiro time delay.

Here, we consider LISA observations of compact galactic binaries in hierarchical systems and identify three main regimes that are governed by the ratio of the outer orbital period to the observation time:

(1) When the outer period is much larger than the observation time, the hierarchical orbit imparts an overall unobservable doppler shift.
(2) When the outer period is up to a factor 10 or so larger than the observation time, the influence of the companion can be detected.
(3) When the outer period is shorter than or comparable to the observation time, the eccentricity and period of the hierarchical orbit can be inferred. In rare cases, a fourth regime can occur.
(4) The acceleration due to the hierarchal perturber can be mistaken for frequency changes due to gravitational wave emission or mass transfer.

This regime occurs when the outer period is larger than the observation time, and the chirp mass and gravitational wave frequency of the compact binary lie in a narrow range of

values. The precise location of the boundaries between the four cases depends on several factors, including the signal-to-noise ratio, the gravitational wave frequency, the mass ratio between the inner binary and the perturber, and the eccentricity of the outer orbit. Using a simple Fisher matrix based estimate for when the frequency change of a nearly monochromatic signal can be detected, we arrive at the condition that, on average, the outer binary can be detected when the period of the outer orbit P_2 obeys the inequality

$$P_2 \lesssim 43.2\ \mathrm{yrs}\left(\frac{\rho}{10}\cdot\frac{m_c}{1.0\ M_\odot}\cdot\frac{f}{5\ \mathrm{mHz}}\right)^{3/4}\left(\frac{m_2}{2\ M_\odot}\right)^{-1/2} \times\left(\frac{T_{\mathrm{obs}}}{4\ \mathrm{yr}}\right)^{3/8}\left(\frac{1+\frac{1}{2}e_2^2}{(1-e_2^2)^{5/2}}\right)^{3/8}. \quad (1)$$

This expression is valid for $P_2 > T_{\mathrm{obs}}$, where T_{obs} is the observation time. For shorter periods, higher derivatives of the frequency change with respect to time need to be accounted for. Other quantities that appear in the expression are the signal-to-noise ratio ρ, the mass of the perturber m_c, the gravitational wave frequency f, the total mass of the system m_2, and the eccentricity of the hierarchical orbit e_2, and we work in geometrical units with $G = c = 1$. To derive this expression, we computed the rms line-of-sight acceleration of the inner binary due to the distant companion, averaging over the orbital period and orientation. Note that some systems will be detectable with longer periods if the orientation and phase of the orbit is more favorable. Also note that LISA is expected to detect hundreds of galactic binaries with signal-to-noise ratios (SNRs) $\rho > 100$ [2], and for these systems, it will be possible to detect systems with $P_2 > 100$ yr.

The outline of the paper is as follows. In Sec. II, we review what is known about compact binaries in hierarchical systems. In Sec. III, we summarize the models and methods used in our study. The orbital model is described in more detail in Sec. IV, and the gravitational wave modeling is outlined in Sec. V. The detectability of hierarchical companions is considered in Sec. VI, and the characterization of the orbits is investigated in Sec. VII. The possibility of confusing the acceleration caused by a distant perturber with orbital evolution due to radiation reaction or mass transfer is discussed in Sec. VIII. We conclude with a summary and discussion of future studies in Sec. IX.

II. COMPACT BINARIES IN HIERARCHICAL SYSTEMS

The majority of stars are members of multiple systems, including binaries, triples, and higher-order hierarchies. The triple fraction is best known for stellar systems with main-sequence components, in particular for lower-mass stars of F and G type where a triple fraction of 11%–20% is found [3,5,24]. There are indications that the triple fraction increases for higher-mass stars as for binaries [25,26]. The period distribution of the inner and outer orbits of triples with F- and G-type primaries are distributed similarly as those of binaries, however, with the additional constraint that the triple is dynamically stable [27]. As a result, the inner orbits tend to be more compact, leading more often to mass transfer episodes and compact binaries [28]. Besides the initial structure of the triple, three-body dynamics can provide additional means to harden the inner binary. The classical low-order quadrupole approximation of the three-body leads to Lidov-Kozai cycles, in which the mutual inclination between the two orbits and the eccentricity of the inner binary vary periodically [8–10]. The octupole terms give rise to the eccentric Lidov-Kozai mechanism, in which even higher eccentricities can be reached [10]. As a result, the (regular and eccentric) Lidov-Kozai mechanism is linked to a variety of exotic astrophysical phenomena, such as stellar mergers in isolated triples [29–33], stellar mergers in binaries near massive black holes [34–38], low-mass x-ray binaries [39–41], blue stragglers [15,42], as well as enhanced dissipation through gravitational wave emission and tides [43,44]. Due to the latter mechanism, also known as high-eccentricity migration or Lidov-Kozai cycles with tidal friction (LKCTF), the inner binary tightens, forming hot Jupiters, e.g., Refs. [45–50], and compact binaries [14,15,43,44]; observationally, roughly 96% of low-mass binaries with periods shorter than 3 days have outer companions [6,7].

In the context of gravitational wave (GW) sources, Lidov-Kozai cycles are relevant, as the gravitational wave inspiral time of a close (inner) binary with compact objects can be significantly reduced, if an outer star is present. Whereas isolated compact binaries need to be formed at periods $\lesssim$0.3 days to merge within a Hubble time, the presence of an outer companion extends the inner period range to hundreds of days if LKCTF is efficient. Even wider inner orbits can be brought to merge or collide if the triple system is weakly hierarchical for which the secular perturbation theory breaks down [17,34,51,52]. Such mergers of compact objects occur in orbits with higher residual eccentricities, e.g., Refs. [53–55].

On the observational side, our knowledge of the triple fraction and orbital structures of triples with compact objects is limited. The highly complete sample of white dwarfs within 20 pc from the Sun contains one to two triples with an inner compact double WD, showing that indeed its possible to form such objects, e.g., Ref. [52]. Moreover, out of about 130 objects in total, there is one confirmed isolated compact double WD and four candidates, indicating that triple sources are relatively abundant.

When shifting our attention from compact double white dwarfs to wide systems, there are only two such binaries within 20 pc. This is in contradiction to theory, from which one would expect 15–30 such systems within 20 pc [52]. As destruction mechanisms (e.g., dynamical interactions or stellar winds) are not efficient enough to explain the

discrepancy, it has been claimed that the progenitor systems are not formed as efficiently as expected, e.g., Ref. [52], or that the wide double white dwarfs have been missed observationally [56]; however, in the state-of-the-art sample of Gaia, no new wide double white dwarfs were found within 20 pc [57].

It is interesting to mention PSR J0337 + 1715, the millisecond pulsar in a hierarchical triple with two white dwarfs [58] with periods of 1.6 and 327 days. As both white dwarfs are low-mass helium dwarfs, the system demonstrates that it is possible in nature for a triple to survive several phases of mass transfer (see, e.g., Refs. [59,60] for possible formation scenarios) and have outer periods in the range of the LISA mission lifetime.

III. SUMMARY OF MODELS AND METHODS

The natural separation of scales found in hierarchical systems allows us to make a number of simplifying assumptions. The few-body Hamiltonian for a hierarchical system can be expanded in the ratio of the semimajor axes yielding terms at monopole, quadrupole, octapole, and higher orders [61–63]. Here, we are mostly interested in 2:1 and 2:2 component hierarchies where the semimajor axis of the binary components is much smaller than semimajor axis of the overall system. Because the hierarchical periods we are considering will be comparable to or larger than the observation time, we can restrict our analysis to the leading order, Newtonian monopole interactions. In this approximation, the motion of the binaries is separate from that of the hierarchical system, and each can be treated as a separate Keplarian system. The center of mass of the inner binary follows a Keplarian orbit around the distant perturber. We are justified in doing this since the Lidov-Kozai [64,65] and eccentric Lidov-Kozai [61,66] oscillations induced by the quadrupole and octapole terms occur on timescales that are long compared to the period of the hierarchical orbit, and very much longer than the observation time. The same is true for the high-order post-Newtonian effects such as periastron precession.

To check that the monopole description is sufficient for our analysis, we can derive qualitative estimate of the contribution of the Lidov-Kozai and eccentric Lidov-Kozai mechanisms on the triple systems under consideration. We compute the variation over the LISA mission lifetime of the inner (e_1) and outer (e_2) eccentricities and the inner ($\imath_1$) and outer ($\imath_2$) inclination angles, due to the combined effect of those two mechanisms. We consider the expressions for the time variation of these physical quantities given in Ref. [10], and in order to obtain rough conservative estimates, we set all geometrical factors (sines and cosines) to unity and then add the absolute value of any additive term in those expressions. From this analysis, we find that the variation over a four year LISA mission duration of the outer inclination angle ($\imath_2$) and the outer eccentricity (e_2) are always negligible, irrespectively of the triple's parameters. Similarly, the change on the values of the inner inclination angle ($\imath_1$) and inner eccentricity (e_1) is always below a few percent, unless we have very small WD masses ($\lesssim 0.2\ M_\odot$), large inner eccentricities ($e_1 \gtrsim 0.3$), and/or low GW frequencies ($f < 1$ mHz). We will leave the investigation of these particular systems to future studies, and in what follows, we will assume the quantities $\imath_1$, e_1, $\imath_2$, and e_2 to be constant. This approximation should work well for the majority of the systems that LISA will be able to observe.

In light of this, we allow for the outer hierarchical orbit to be eccentric but make the further simplifying assumption that the inner orbit responsible for the gravitational wave emission is circular. We can justify this choice in two ways. First, gravitational radiation acts to quickly circularize orbits, and second, even if effects such as Lidov-Kozai oscillations have managed to maintain the eccentricity of the inner binary, our results will be little changed, at least for moderate eccentricities. The reasoning is as follows: for slowly evolving, moderately eccentric systems, the gravitational wave signal can be expressed as a sum of circular binaries with periods at harmonics of the orbital period. The separation of these harmonics in frequency is very much larger than the sidebands imparted by the hierarchical orbit, so there is zero confusion between the two effects. The sum of circular binary signals for an eccentric system contains information almost identical to that of a single circular binary for the purposes of the current analysis, so in the interests of computational efficiency, we neglect the eccentricity of the inner binary. To verify this argument. we model a triple system with nonzero inner eccentricity and perform parameter estimation by obtaining the marginalized posteriors for the outer orbit parameters. We compare the posteriors to those for the exact same system but with zero inner eccentricity and find that the posteriors are identical, hence demonstrating that the presence of sidebands due to eccentricity of the inner orbit will not affect our results—see the end of Sec. VII for details.

To assess the detectability of the distant companion and the accuracy with which the parameters of the orbits can be inferred, we use a mixture of methods. To make quick estimates and derive analytic scalings, we compute Fisher information matrices, and to spot check these estimates and provide more detailed results, we employ Bayesian inference via the Markov Chain Monte Carlo algorithm.

IV. HIERARCHICAL ORBIT MODEL

In this section, we derive how the perturbing companion affects the center-of-mass motion of the inner binary in the hierarchical orbit which will impart perturbations to the gravitational waveform. We desire to extract the line-of-sight component of the inner binary's center-of-mass velocity. For an isolated binary, its center of mass is stationary with respect to the solar system barycenter (ignoring unobservable constant peculiar velocities), but

this line-of-sight component of the induced center of mass will create a time-dependent redshift as seen in the barycenter frame. We will use "1" subscripts to denote orbital parameters of the inner gravitational wave emitting binary composed of masses m_a and m_b for a total mass of m_1. The subscript "2" will denote the Keplerian outer orbit describing the motion of the perturber m_c and the monopole mass of the inner binary. In our hierarchical approximation, in which we essentially have a circular Keplerian orbit emitting a gravitational wave visible to LISA inside of a larger outer Keplerian orbit that is governed by

$$\mathbf{a}_2 = -\frac{Gm_2}{r_2^2}\hat{\mathbf{r}}_2, \tag{2}$$

where $\mathbf{a}_2$ is the relative acceleration and $\hat{\mathbf{r}}_2 = \hat{\mathbf{r}}_c - \hat{\mathbf{r}}_1$ is the unit separation vector as defined in an inertial coordinate system of the triple and $m_2 = m_a + m_b + m_c$.

The solution for the orbital motion is then

$$\mathbf{r}_2(t) = r_2(t)(\cos\varphi_2, \sin\varphi_2, 0), \tag{3}$$

where

$$r_2(t) = \frac{a_2(1-e_2^2)}{1 + e_2\cos\varphi_2}, \tag{4}$$

defining the standard Keplerian ellipse. The quantities introduced are defined as follows: φ_2 is the orbital phase of the outer orbit and e_2 and a_2 are its eccentricity and semimajor axis respectively. To relate the orbital phase to time, it is convention to introduce the eccentric anomaly. The eccentric anomaly is an angle related to the orbital phase through the geometric equation

$$\varphi = \varphi_0 + 2\tan^{-1}\left(\sqrt{\frac{1+e}{1-e}}\tan\frac{u}{2}\right), \tag{5}$$

where u is the eccentric anomaly. The eccentric anomaly is then related to time through Kepler's equation

$$n_2(t - T_2) = u_2 - e_2\sin u_2, \tag{6}$$

where $n_2 = \sqrt{m_2/a_2^3}$ defines the mean motion, or mean angular frequency associated with an orbit. The mean motion is related to P_2, the outer period, $n_2 = 2\pi/P_2$, and lastly the parameter T_2 is the time of pericenter passage, a constant of integration.

The desired velocity of the inner binary's center of mass is simply obtained by $\mathbf{v}_1 = (m_c/m_2)\mathbf{v}_2$, and differentiating Eq. (3)

$$\mathbf{v}_1 = \frac{m_c}{m_2}\sqrt{\frac{Gm_2}{p_2}}(-\sin\varphi_2, \cos\varphi_2 + e_2, 0), \tag{7}$$

where $p_2 = a_2(1-e_2^2)$ is the semilatus rectum. Up to this moment, we have been working in a coordinate system where the outer orbit defines the xy-plane. We must rotate our system to properly orient it into the coordinate system used by our detector model: the Solar System barycenter frame. This may be accomplished through a series of Euler rotations: a rotation of $-\omega_2$, around the barycenter's z axis, then by $-\iota_2$ around the new x axis, and finally $-\Omega_2$ around the new z axis, which are given by the matrices

$$\mathbb{R}_1 = \begin{pmatrix} \cos\omega_2 & -\sin\omega_2 & 0 \\ \sin\omega_2 & \cos\omega_2 & 0 \\ 0 & 0 & 1 \end{pmatrix}, \tag{8}$$

$$\mathbb{R}_2 = \begin{pmatrix} 1 & 0 & 0 \\ 0 & \cos\iota_2 & -\sin\iota_2 \\ 0 & \sin\iota_2 & \cos\iota_2 \end{pmatrix}, \tag{9}$$

$$\mathbb{R}_3 = \begin{pmatrix} \cos\Omega_2 & -\sin\Omega_2 & 0 \\ \sin\Omega_2 & \cos\Omega_2 & 0 \\ 0 & 0 & 1 \end{pmatrix}, \tag{10}$$

operated in the order $\mathbb{R} = \mathbb{R}_3 \cdot \mathbb{R}_2 \cdot \mathbb{R}_1$. As shown in Fig. 1, the line of ascending nodes (labeled in the figure) is defined by a rotation of angle Ω_2 from the barycenter x axis to where the outer orbital plane intersects the ecliptic. The angle ω_2 defines the rotation angle from the line of nodes to the argument of periapsis (the position of which is given by the solid line passing through the semimajor axis of the orbit), and ι_2 is the inclination angle, i.e., the angle between the outer orbit's angular momentum $\hat{L}_2$ and the z axis of the barycenter coordinates (here neglecting any contribution to

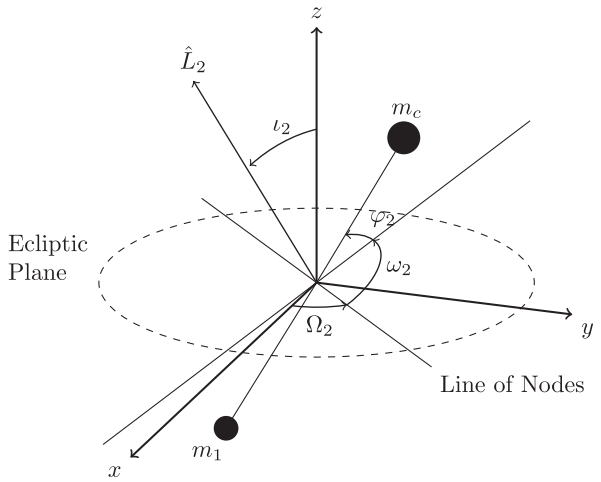

FIG. 1. The geometry of the outer orbit consisting of m_c and the inner binary's monopole moment m_1 as displayed above, where the orientation angles are with respect to the solar system barycenter frame with the z axis normal to the plane of the ecliptic.

angular momentum due to the fact that the inner binary is extended and has an orbit of its own). Note that here that $\cos\iota_1 = \hat{n}\cdot\hat{L}_1$ defines the inner binary's inclination with respect to the line of sight.

Finally, we may construct the desired quantity: the line-of-sight velocity $v_\parallel$. We can use the line-of-sight vector $\hat{\mathbf{n}}$ pointing from the origin of the barycenter coordinates to the triple center of mass. Due to the large distances involved, we will assume that the sky location (θ, ϕ) of the inner binary and of the triple's center of mass are located at the same point on the sky. This vector is given by $\hat{\mathbf{n}} = (\sin\theta\cos\phi, \sin\theta\sin\phi, \cos\theta)$. At last, we obtain the expression

$$v_\parallel(t) = \hat{\mathbf{n}}\cdot\mathbb{R}\cdot\mathbf{v}_1, \tag{11}$$

$$= \hat{\mathbf{n}}\cdot\mathbb{R}\cdot\left(\frac{m_c}{m_2}\mathbf{v}_2\right),$$

$$= \frac{m_c}{m_2}\sqrt{\frac{Gm_2}{p_2}} \times \{C(\theta,\iota_2,\phi-\Omega_2)[\cos(\varphi_2+\omega_2)+e_2\cos\omega_2] - S(\theta,\phi-\Omega_2)[\sin(\varphi_2+\omega_2)+e_2\sin\omega_2]\}, \tag{12}$$

where $C(\theta,\iota_2,\phi-\Omega_2) = \cos\theta\sin\iota_2 + \sin\theta\cos\iota_2\sin(\phi-\Omega_2)$ and $S(\theta,\phi-\Omega_2) = \sin\theta\cos(\phi-\Omega_2)$. In the above form, it is unclear how many extra parameters are truly involved in the modeling of the triple system, so we rewrite the line-of-sight velocity in the simpler form

$$v_\parallel(t) = \mathcal{A}_2[\sin(\varphi_2+\varpi)+e_2\sin(\varpi)], \tag{13}$$

where $\mathcal{A}_2 = \frac{m_c}{m_2}\sqrt{\frac{m_2}{p_2}}\bar{A}$ and $\bar{A}^2 = C^2+S^2$ and finally $\varpi = \omega+\bar{\phi}$, where $\tan\bar{\phi} = \frac{C}{-S}$. With the line-of-sight velocity written this way, we can see what combination of parameters can be measured. To specify $v_\parallel(t)$, we needed the parameters n_2, e_2, T_2, ι_2, ω_2, Ω_2, m_c, and m_2 (note that the sky location angles are part of the binary model), but unfortunately we do not have access to all of these parameters due to degeneracies in the model which can be seen from Eq. (13). The parameters ω_2, Ω_2, and ι_2 get lumped into $\mathcal{A}_2$ and ϖ, leaving us in no position to parse the dynamically interesting ι_2 from other orientation angles. This amplitude has an average value of roughly 0.77, which will be used in the analysis contained in later sections. Also, hidden in $\mathcal{A}_2$ are m_2 and m_c, which we will not have access to individually. The orbital phase φ_2 contains the uninteresting parameter T_2 and is also controlled strongly by the mean motion n_2 and eccentricity e_2 parameters. We are now in a position to incorporate the line-of-sight velocity into the gravitational waveform. For eclipsing systems, the Shapiro time delay can break some of the degenerates and allow us to measure ι_2. We will leave the analysis of the gravitational wave Shapiro time delay to future work.

V. GRAVITATIONAL WAVE AND INSTRUMENT MODEL

We will first briefly review the gravitational wave model for an isolated galactic binary as seen by LISA and then incorporate the effects due to the companion body. These are low-mass binaries which are millions of years away from merging, and therefore we will only be capturing them in the inspiral phase. The plus and cross gravitational wave polarizations in the compact binary's barycenter frame are given by

$$h_+ = \frac{2\mathcal{M}}{D_{\rm L}}(\pi f_{\rm gw}(t))^{2/3}(1+\cos^2\iota_1)\cos\Psi_{\rm gw}, \tag{14}$$

$$h_\times = -\frac{4\mathcal{M}}{D_{\rm L}}(\pi f_{\rm gw}(t))^{2/3}\cos\iota_1\sin\Psi_{\rm gw}, \tag{15}$$

where $D_{\rm L}$ is the luminosity distance, $\mathcal{M} = (m_a m_b)^{3/5}/m_1^{1/5}$ is the chirp mass, $f_{\rm gw}$ is the instantaneous gravitational wave frequency (as measured in the compact binary's barycenter frame), $\Psi_{\rm gw}$ the corresponding gravitational wave phase, and lastly ι_1 is the inclination of the inner binary, i.e., $\cos\iota_1 = \hat{L}_1\cdot\hat{n}$. One may obtain the gravitational wave phase from the frequency through $\Psi_{\rm gw} = 2\pi\int^t f_{\rm gw}(t')dt' + \phi_0$ where ϕ_0 is an arbitrary phase shift.

A. Numerical implementation

For galactic binaries of which the orbital evolution is dominated by the gravitational wave radiation reaction, the frequency evolution is given by

$$f_{\rm gw}(t) = \frac{1}{8\pi\mathcal{M}}\left(\frac{5\mathcal{M}}{t_c-t}\right)^{3/8}, \tag{16}$$

where t_c is the time of coalescence for the binary; a 3 mHz, 0.265 $M_\odot$ galactic binary will merge in one million years. The number of $1/T_{\rm obs}$ frequency bins a fiduciary source evolves through over the LISA mission lifetime is given by [67]

$$\dot{f}T_{\rm obs}^2 = 5.1\left(\frac{\mathcal{M}}{0.32\ M_\odot}\right)^{5/3}\left(\frac{f}{5\ \rm mHz}\right)^{11/3}\left(\frac{T_{\rm obs}}{4\ \rm yrs}\right)^2 \tag{17}$$

$$\ddot{f}T_{\rm obs}^3 = 1.5\times10^{-4} \times\left(\frac{\mathcal{M}}{0.32\ M_\odot}\right)^{10/3}\left(\frac{f}{5\ \rm mHz}\right)^{19/3}\left(\frac{T_{\rm obs}}{4\ \rm yrs}\right)^3. \tag{18}$$

The strong frequency dependence in these expression implies that the higher frequency sources will have more measurable chirps. It is this frequency dependence that will

allow us to determine the physics responsible for the evolution of a population of binaries. A similar order of magnitude frequency evolution is experienced by galactic binaries which involve stable mass transfer [68]. A key difference is that mass transfer tends to widen orbits leading to a frequency decrease over time. The mild evolution in gravitational wave frequency lends itself to a Taylor expansion,

$$f_{\rm gw} = f + \dot{f}t + \frac{1}{2}\ddot{f}t^2, \tag{19}$$

the coefficients of which are determined by the dynamics at play in the binary. We shall refer to f (and the equivalently redshifted version during the triples discussion) as the carrier frequency.

Cornish and Littenberg [69] present a frequency domain model for galactic binaries measured by LISA. Under the rigid adiabatic approximation to the LISA motion, one is able to perform a fast-slow decomposition, due to the slowly evolving amplitude (varying on timescales of a year mostly due to LISA's motion) and the fast varying phase due the larger carrier frequency (corresponding to orbital periods of minutes to hours for galactic binaries) of the waveform allowing a rapid evaluation of the waveform, specifically the time-delay interferometry (TDI) variables X, Y, and Z (where tildes over these variables will denote their Fourier transform). Through a linear superposition, these data channels form noise-orthogonal variables A, E, and T [70] (of which only A and E will be sensitive to the triple systems of interest).

The presence of a perturbing companion star m_c leads to an acceleration of the center of mass with respect to the barycenter frame, hence redshifting the signal such that the gravitational wave phase gets modified,

$$\Psi_{\rm gw} = 2\pi \int^t [1 + v_\parallel(t')] f_{\rm gw}(t') dt' + \phi_0, \tag{20}$$

where $v_\parallel$ is the line-of-sight velocity obtained in the previous section.[1] In Fig. 2, the quantity h_+ (normalized to 1) is displayed for a circular triple system of which the outer period was chosen to be very short to exaggerate the effects. The frequency oscillates around the carrier frequency f modulating the gravitational wave phase.

To account for the aforementioned differences between an isolated galactic binary and a triple, the Cornish & Littenberg code [69] must be modified. To properly calculate the gravitational wave transfer function, one must evaluate it at the gravitational wave frequency observed by the LISA detectors. The Taylor expanded frequency evolution [as in Eq. (19)] is redshifted with respect to the solar system barycenter, i.e., $f_{\rm gw} \to (1 + v_\parallel) f_{\rm gw}$. The line-of-sight velocity is numerically obtained through Eq. (13) and the inversion of Kepler's equation. For the isolated galactic binaries, the gravitational phase may be easily integrated. When this binary resides in a triple system, an extra term in the gravitational wave phase integral crops up $2\pi \int v_\parallel f_{\rm gw} dt$, which is numerically integrated, interpolated at the detector sampling intervals, and then appended to the isolated galactic binary gravitational wave phase. These modifications to the gravitational wave frequency get applied to the slow portion of the waveform model, which is sampled at cadence much longer than the orbital period.

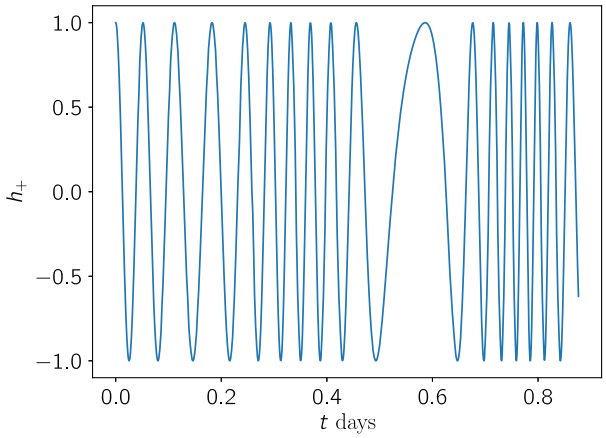

FIG. 2. The gravitational waveform seen at the solar system barycenter for a system with outer period $P_2 = 1.1$ hr and the line-of-sight velocity amplitude 0.1. The carrier frequency f of the gravitational wave in this example is 5 mHz. The strain amplitude has been normalized to 1 such that the only time dependence crops up in the gravitational wave phase. The frequency of the oscillations is clearly changing.

The log likelihood function used in our analysis involves noise-weighted inner products of the form

$$(g|k) = 4\mathcal{R} \int_0^\infty \frac{\tilde{g}^*(f)\tilde{k}(f)}{S_n(f)} df, \tag{21}$$

where g and k are arbitrary waveforms as seen by LISA and $S_n(f)$ is the one-sided noise power spectral density. Further discussion of this quantity and the noise model for LISA, including both instrumental noise and unresolved galactic binary confusion noise, can be found in Refs. [2,71,72]. The SNR ρ is defined as $\rho^2 = (h|h)$ for a given waveform h.

Examples of the frequency domain strain amplitude can be found in Figs. 3 and 4. Both of these waveforms were generated for inner binaries with $f = 5$ mHz and a chirp mass of 0.32 $M_\odot$ (which fixes the source frame frequency evolution as determined by General Relativity) for a four

[1]Note that there should be an additional correction to Eq. (20) due to the fact that time in the two frames is related by $t \mapsto t + r_\parallel/c$. This correction is, however, negligible for the triple systems considered in this work, but it might be relevant for systems closer to coalescence, e.g., hierarchical triple black hole systems observable with LISA.

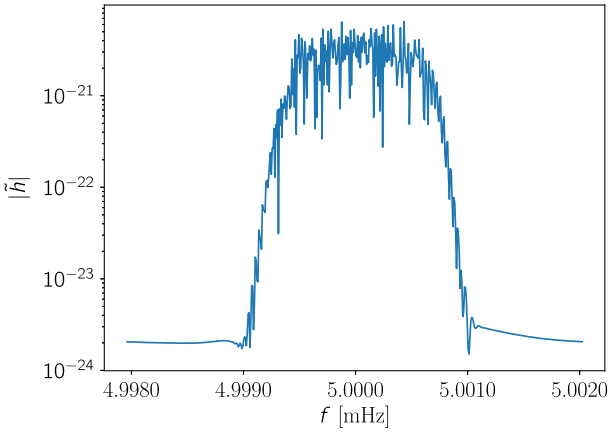

FIG. 3. The X TDI channel is displayed for a triple system with an outer orbital period $P_2 = 1.5$ yr and $e_2 = 0.3$. The presence of the perturbing companion induces harmonics of the carrier frequency and of the harmonics present due to LISA's modulations. The amplitude (therefore, distance) of the system was modified to give a SNR of 20. The other parameters of this system were chosen as follows: $\dot{f} = 1.11 \times 10^{-15}$, $\theta = 1.52$, $\phi = 4.577$, $\phi_0 = 0.346$, and $\psi = 1.58$. The masses were chosen as $m_a = 0.6\ M_\odot$, $m_c = 1.0\ M_\odot$, and $\mathcal{M} = 0.32\ M_\odot$. The observation period for this figure was four years.

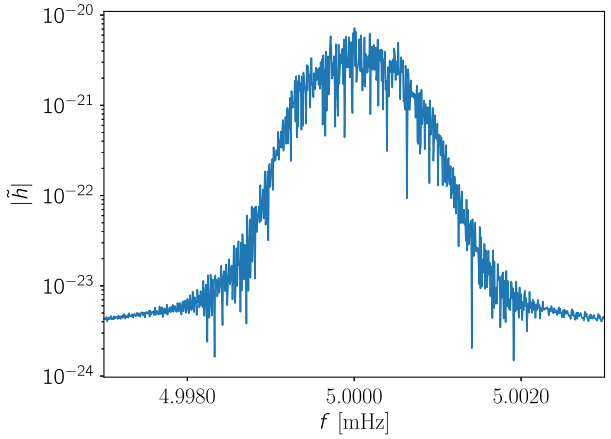

FIG. 4. The X TDI channel is displayed for triple system with an outer orbital period $P_2 = 0.6$ yr and $e_2 = 0.7$. In this example, the harmonics induced by the companion star and LISA are interfering. Eccentricity in the outer orbit changes the distribution of power in the triple induced harmonics. The other parameters were chosen to be the same as in Fig. 3.

year observation period at a 15 sec cadence. In Fig. 3, the outer orbit revolves every 1.5 years and has an eccentricity of 0.3. An isolated binary is nearly monochromatic, resulting in a near delta function in the frequency domain but, due to the modulations caused by the cartwheel motion of the LISA observatory around the Sun, picks up sidebands of which the phase and relative amplitude are determined by the sky location and gravitational wave polarization of the binary. The introduction of a perturbing

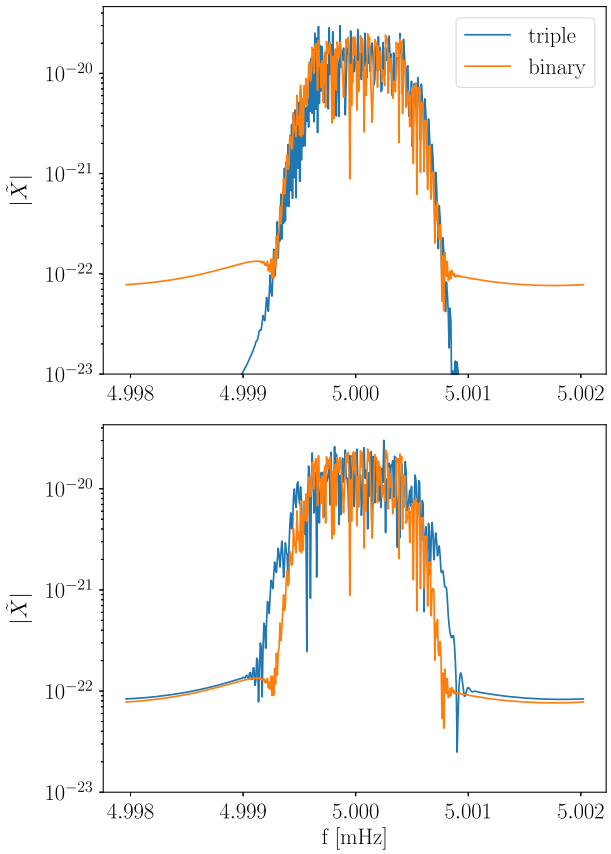

FIG. 5. The TDI X-channel response for isolated binary signals—denoted in orange—and for triple signals—colored blue. The SNRs of these signals were chosen to be 20 and were observed for four years. The outer eccentricity of the triple signals was set to 0.3. The outer period in the upper figure is 100 years (much larger than observation period) and in the lower figure is 3.6 years (comparable to observation period). The other parameters are identical to those chosen for Fig. 3.

third body generates more harmonics of the frequencies already present and tends to increase the bandwidth of the signal. Increasing the eccentricity of the outer orbit shifts the distribution of power into higher modes of the triple harmonics.

In Fig. 4, the system has a tighter outer period of 0.6 years and a larger eccentricity of 0.7. Here, the orbital period P_2 is comparable to the orbital timescale of LISA, leading to a strong interference of harmonics. The sidebands of the carrier frequency induced by the triple are now more widely spaced than those imparted by LISA orbit, leading to a much broader signal, which is amplified by the larger eccentricity. If one were to consider a system of an even shorter period, then the triple induced harmonics separate out into isolated sidebands.

One can gain insight visually into our ability to distinguish a triple system from a binary by considering Fig. 5. In both panels, the blue lines represent the power in the X TDI channel for an isolated binary signal, and orange

represents the same data channel for a triple system where the parameters characterizing the inner binary are the same for all signals displayed in this figure. The orange lines are therefore signals of the same system in both panels. The blue lines differ from each other purely in their outer orbital period. These signals are the result of a four year observation period. In the regime where the outer period is much larger than the observation period, we are still able to measure the frequency evolution of the signal. This is seen in the upper panel of Fig. 5, where the outer orbital period was set to 100 years. Considering the triple signal in relation to the binary signal you can see that the redshifting through the rightward shift in frequency of the triple signal. For this very large outer period, one might in fact mistake this signal for an isolated binary with slightly different parameters than those in the actual inner binary. In the lower panel, we see a more severe difference since the outer orbital period was set to 3.6 years, comparable to the observation period. There is a severe broadening of the signal, and the power structure is vastly different than that seen in the upper panel. This difference allows us to detect the presence of the triple and characterize the parameters of the outer orbit, which will be demonstrated later.

B. Eccentric inner binary signal

In order to demonstrate that the presence of gravitational wave harmonics due to an eccentric inner binary, $e_1 \neq 0$, does not affect the characterization of the outer orbit, we extend the waveform model to cover inner binaries with moderate eccentricity. The gravitational wave plus and cross polarizations at Newtonian order for eccentric binaries are given by

$$h_{+,\times} = -\frac{m_1\eta_1}{D_L}(2\pi m_1 F_1)^{2/3}\sum_{j=1}^{\infty}[C^{(j)}_{+,\times}(e_1,\beta_1,\iota_1)\cos jl_1 + S^{(j)}_{+,\times}(e_1,\beta_1,\iota_1)\sin jl_1], \tag{22}$$

where $\eta_1 = m_a m_b/m_1^2$ is the symmetric mass ratio, F_1 is the mean orbital frequency, β_1 defines the pericenter angle, and ι_1 is the inclination angle of the inner binary. The sum is over harmonics of the gravitational wave signal, and the coefficients $C^{(j)}_{+,\times}$ and $S^{(j)}_{+,\times}$ are the amplitudes of these harmonics. Their functional form is given by Moore *et al.* [73].

For mild eccentricities, the second harmonic is dominant, and the frequency associated with it is Taylor expanded as in Eq. (19),

$$f^{j=2}_{\rm gw} = f + \dot{f}t + \frac{1}{2}\ddot{f}t^2. \tag{23}$$

In order to calculate the other harmonics, we make use of the Cornish and Littenberg galactic binary waveform generator, but with the following harmonic dependent conditions:

(1) The gravitational wave frequency seen gets modified by $f^{j}_{\rm gw} \to \frac{j}{2} f^{j=2}_{\rm gw}$.
(2) Similarly, the phase must be modified $\Psi^{j}_{\rm gw} \to \frac{j}{2}\Psi^{j=2}_{\rm gw}$.

The amplitudes of the TDI variables were then modulated by the harmonic coefficients. For these eccentric waveforms, we keep the first four harmonics in our analysis, which is enough to maintain 99% of the gravitational wave power up to $e_1 = 0.2$ (as determined by the harmonic coefficients). There is an important feature to keep in mind about the structure of the gravitational wave signal. The harmonics are separated by $\Delta f = f_1$ Hz, which for a 1.5 mHz orbital frequency corresponds to 47 000 frequency bins for a one year observation period. The bandwidth for these harmonics is at most a couple thousand bins, which tells us that the harmonics are well separated and do not interfere with each other, nor do the harmonics due to the eccentricity overlap in any way with the harmonics imparted by a hierarchical companion. This is why we are justified in neglecting any eccentricity of the inner binary and using the simpler circular orbit model. This argument is confirmed by simulations in Sec. VII.

VI. DETECTING HIERARCHICAL COMPANIONS

When LISA first detects a triple, only the intrinsic gravitational wave frequency of the inner binary will be measurable. As more cycles are accumulated, and the center of mass of the inner binary has moved through a significant portion of the outer orbit, the data will support the inclusion of orbitally induced redshifts. We will now estimate when we expect the frequency evolution to be measurable; i.e., for a given source and observation period and an average oriented source, what P_2's will we be able to detect with the effect of this center-of-mass motion?

From the gravitational wave phase quoted in Eq. (20), it is straightforward to obtain the time derivative of the frequency in the barycenter frame for a binary in a triple system which has negligible source frame frequency evolution

$$\dot{f} = a_{1,\parallel} f, \tag{24}$$

where $a_\parallel$ is the line-of-sight acceleration of the inner binary's center of mass. The line-of-sight acceleration can be obtained by differentiating Eq. (7)

$$\mathbf{a}_1 = -\frac{m_c}{p_2^2}(1+e_2\cos\varphi_2)^2(\cos\varphi_2, \sin\varphi_2, 0), \tag{25}$$

rotating the resulting vector by applying the rotation matrices, and projecting the rotated vector along the line-of-sight. This gives

$$a_{1,\parallel} = -\frac{m_c}{p_2^2}(1+e_2\cos\varphi_2)^2 \times [S\cos(\omega_2+\varphi_2) + C\sin(\omega_2+\varphi_2)], \tag{26}$$

where S and C are defined as before; cf. Eq. (12). We would like to consider the average magnitude of this acceleration for a given orientation and sky location. We may square this quantity and then average it over the angles ϕ, θ, ω_2, and ι_2,

$$\langle a_{1,\parallel}^2 \rangle = \frac{1}{(4\pi)^2}\int_0^{2\pi} d\phi \int_{-1}^{1} d(\cos\theta) \times \int_0^{2\pi} d\omega_2 \int_{-1}^{1} d(\cos\iota_2) a_{1,\parallel}^2 \tag{27}$$

$$= \frac{m_c^2}{3p_2^4}(1+e_2\cos\varphi_2)^4. \tag{28}$$

To calculate the rms acceleration, we average the previous result over the course of an orbit,

$$a_{\parallel \mathrm{RMS}}^2 = \frac{1}{P_2}\int_0^{P_2} \langle a_{1,\parallel}^2 \rangle dt \tag{29}$$

$$= \frac{1}{P_2}\int_0^{P_2} \langle a_{1,\parallel}^2 \rangle \dot{\varphi}_2^{-1} d\varphi_2 \tag{30}$$

$$= \frac{m_c^2}{3m_2^{4/3}}\left(\frac{2\pi}{P_2}\right)^{8/3} \frac{1+\frac{1}{2}e_2^2}{(1-e_2^2)^{5/2}}. \tag{31}$$

In the regime that $P_2 > T_{\mathrm{obs}}$, we may Taylor expand the gravitational wave frequency. Equation (24), when averaged over angles and over an orbit, provides us with a rough estimate of the size of $\dot{f}$ for an average outer orbit orientation which started at an average spot in its orbit when LISA began to collect data. With this, we can ascertain how many frequency bins this $\dot{f}$ estimate will evolve the carrier frequency through,

$$\dot{f}T_{\mathrm{obs}}^2 = 573\left(\frac{P_2}{1\ \mathrm{yr}}\right)^{-4/3}\left(\frac{m_c}{1\ M_\odot}\right)\left(\frac{m_2}{2\ M_\odot}\right)^{-2/3} \times \left(\frac{T_{\mathrm{obs}}}{4\ \mathrm{yr}}\right)^2\left(\frac{f}{5\ \mathrm{mHz}}\right)\sqrt{\frac{1+\frac{1}{2}e_2^2}{(1-e_2^2)^{5/2}}}. \tag{32}$$

In order to ascertain when this effect is measurable, we utilize Fisher matrix estimates for the error in measurement of $\dot{f}$. The Fisher matrix, by the Cramer-Rao bound, provides an estimate of the covariance matrix (upon inversion of the Fisher matrix), thereby providing error estimates. The Fisher matrix is defined as

$$\mathbf{\Gamma}_{ij} = (h_{,i}|h_{,j}), \tag{33}$$

where $h_{,i}$ are derivatives of the waveform with respect to parameter λ^i and then evaluated at the true parameters. For a triple signal of which the outer period is larger than LISA's observation period, we may readily approximate the frequency evolution of the system by a Taylor expansion as we would for a mildly chirping isolated binary. This allows us to utilize the fast galactic binary waveform to calculate the Fisher matrix.

Seto [67] used a simple toy model for a Fisher matrix analysis to estimate the measurement errors in some of the galactic binary parameters. In the Appendix, we expand upon these results and investigate how the errors get inflated by including more parameters through the use of the full galactic binary model. We find that the $\dot{f}$ and $\ddot{f}$ errors become inflated through the inclusion of the full set of galactic binary parameters. The criterion which we use to determine whether $\dot{f}$ is a measurable parameter is that $\dot{f}$ must be larger than 3σ (as estimated by the Fisher matrix) compared to no frequency evolution at all. This yields the expression quoted in Eq. (1) in the Introduction, which we repeat here for completeness:

$$P_2 \lesssim 43.2\ \mathrm{yrs}\left(\frac{\rho}{10}\cdot\frac{m_c}{1.0\ M_\odot}\cdot\frac{f}{5\ \mathrm{mHz}}\right)^{3/4}\left(\frac{m_2}{2\ M_\odot}\right)^{-1/2} \times \left(\frac{T_{\mathrm{obs}}}{4\ \mathrm{yr}}\right)^{3/8}\left(\frac{1+\frac{1}{2}e_2^2}{(1-e_2^2)^{5/2}}\right)^{3/8}. \tag{34}$$

A fiducial source with an outer orbital period of 40 years would have a measurable frequency evolution by the time the nominal LISA mission concluded. When the outer eccentricity reaches $e_2 = 0.7$, the outer periods is measurable out to $P_2 = 110$ yr for typical systems. We see that for larger companion masses (assuming fixed total mass m_2) the larger the outer period we can measure. Thus, we see an increase in the detectability of triples with large companion masses. The opposite is true as we increase the total mass.

We may make similar applications of the Fisher analysis to ascertain when the gravitational wave carrier frequency becomes biased (i.e., differs from the source frame value in a measurable way) for a given P_2. The rms line-of-sight velocity is given by

$$v_{\parallel \mathrm{RMS}}^2 = \frac{m_c^2}{3m_2^{4/3}}\left(\frac{2\pi}{P_2}\right)^{2/3}, \tag{35}$$

such that when

$$P_2 \lesssim 71.8\ \mathrm{yrs}\left(\frac{\rho}{10}\cdot\frac{m_c}{1.0\ M_\odot}\cdot\frac{f}{5\ \mathrm{mHz}}\right)^{3} \times \left(\frac{m_2}{2\ M_\odot}\right)^{-2}\left(\frac{T_{\mathrm{obs}}}{4\ \mathrm{yrs}}\right)^{3} \tag{36}$$

our measurements of the carrier frequency f will be biased. This is potentially the most concerning result if one is interested in the orbital period distribution of the galactic binaries, as for sources which only have f measured, this yields a quite large range of outer orbital periods which could bias the frequency measurement.

Another question of interest is when the parameter $\ddot{f}$ is measurable (recall that here we are only considering the frequency evolution coming from the center-of-mass motion). Upon measuring f, $\dot{f}$, and $\ddot{f}$, we have the best chance of determining the underlying physics for mildly evolving sources. The rms jerk is given by

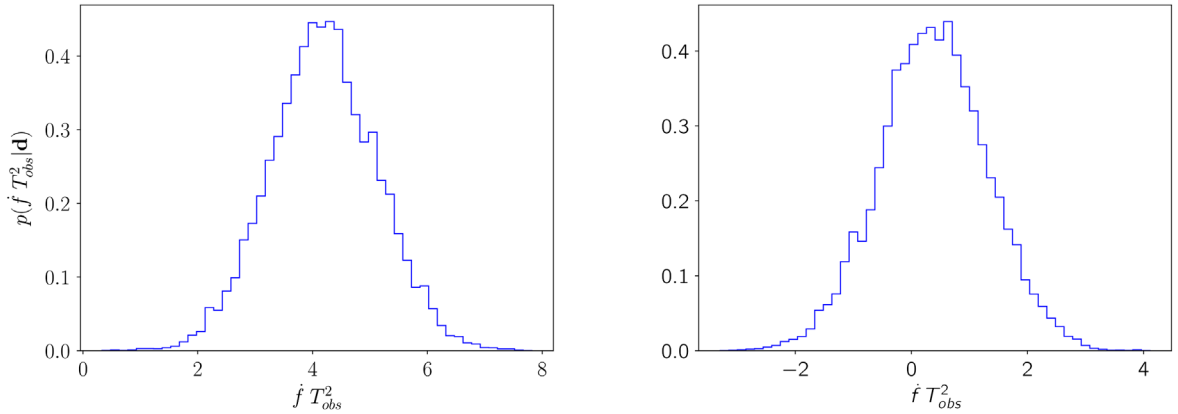

FIG. 6. Here, we display the posteriors for the parameter $\dot{f}T^2_{\rm obs}$ marginalized over all other system parameters. The simulated systems had a total mass of $m_2 = 1.77\ M_\odot$, with $\mathcal{M} = 0.32\ M_\odot$, $\rho = 20$, and an observation period of one year. The time of pericenter passage for the left-hand figure was set to 0, while for the right-hand side, T_2 was set to $-P_2/8$, i.e., an eighth of an orbit. The remaining parameters $\dot{f}$, θ, ϕ, ψ, and ϕ_0 have been set to those chosen in Fig. 3.

$$\dot{a}^2_{\parallel \rm RMS} = \frac{m_c^2}{3m_2^{4/3}}\left(\frac{2\pi}{P_2}\right)^{14/3}\frac{1+\frac{19}{2}e_2^2+\frac{69}{8}e_2^4+\frac{9}{16}e_2^6}{(1-e_2^2)^{11/2}}, \quad (37)$$

which for fiduciary values becomes measurable when

$$P_2 \lesssim 16.7\ \text{yrs}\left(\frac{\rho}{10}\cdot\frac{m_c}{1.0\ M_\odot}\cdot\frac{f}{5\ \text{mHz}}\right)^{3/7} \times \left(\frac{m_2}{2\ M_\odot}\right)^{-2/7}\left(\frac{T_{\rm obs}}{4\ \text{yrs}}\right)^{3/7}. \quad (38)$$

To verify the validity of the preceding results, based on a Fisher matrix analysis, we now spot check the measurability of the frequency evolution of a triple system using Markov Chain Monte Carlo (MCMC) simulations. Simulated data were produced for a triple system and analyzed using the Taylor expanded frequency evolution model. The MCMC consisted of a burn-in phase such that the galactic binary model could search through parameter space to identify a regime in which the triple signal was described well by the binary model. A mixture of the Fisher matrix proposal, differential evolution proposals, and draws from the prior distribution were utilized to explore the posterior distribution [74,75]. Since we have developed a quick numerical model to generate the signal from these triple systems, the proposal distributions may choose any parameters randomly, and we can generate a model for those parameters on the spot. Parallel tempering was also used to ensure a wide exploration of parameter space and to move between secondary modes of the posterior.

In Fig. 6, the posteriors for the parameter $\dot{f}$ (marginalized over all other parameters) are displayed for two triple systems. The outer period was chosen to be 46 years, i.e., the value obtained from the relation (1) using the modified triple parameters. The errors predicted by the Fisher matrix for $\dot{f}$ are a bit smaller compared to the error measured by the MCMC, suggesting that we might be marginally overestimating the outer periods we can confidently measure. The difference between these two posteriors is the time of pericenter passage T_2 which differed by an eighth of an orbit between the two systems. This demonstrates that it is very important where we catch the triple in its orbit when LISA turns on, as the measurability of $\dot{f}$ is quite sensitive to T_2. This is especially important point to consider for larger outer period sources. Here, we have seen that the Fisher analysis has roughly identified the regime in which we may hope to identify the presence of a triple system depending on where in the orbit we are measuring the gravitational wave signal.

VII. CHARACTERIZING THE HIERARCHICAL ORBIT

Now that we have ascertained when the effects of a triple system are detectable, we would like to know when the parameters of the triple orbit can be measured. To determine this, we utilized the Fisher information matrix for the triple signal. The criterion that we use to determine if a parameter is measurable is as follows: if the error in a parameter, as estimated by the Fisher matrix, is less than 50% of its true value, then we claim this parameter can be measured. For triple systems, the best measured parameter pertaining to the outer orbit is the outer orbital period, and if this quantity can be measured, we say that the triple can be characterized (at least to some level).

In Fig. 7, we display the results of the Fisher matrix based analysis. Systems with carrier frequencies and outer periods in the shaded region have orbits of which the parameters *cannot* be measured. To determine the separating line, we construct a system with a given carrier frequency f and a very short outer period P_2 and estimate its error with a Fisher analysis. The outer orbital is gradually made larger until its effects on the gravitational

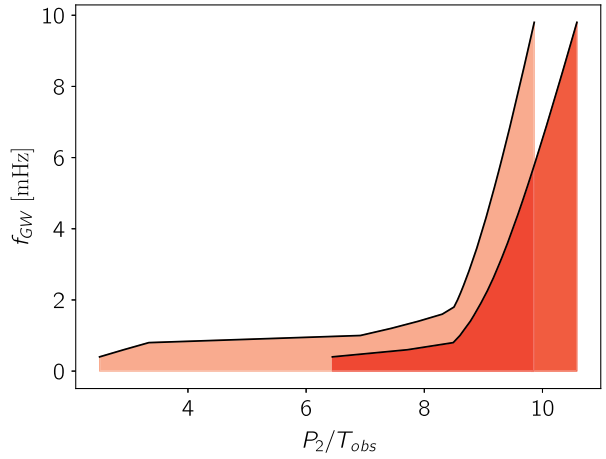

FIG. 7. The shaded regions denote triple systems which cannot have their outer orbital parameters measured. In other words, systems to the right of the shaded regions can have at least the outer orbital period determined. Note the orbits period P_2 is given in units of the observation time $T_{\rm obs}$, which could be as large as ten years. The left black line is for a SNR 20 system, and the right line is for SNR 100. This system had the parameters $m_2 = 2.0\ M_\odot$, $m_c = 1.0\ M_\odot$, $m_a = 0.5\ M_\odot$, and $\mathcal{M} = 0.32\ M_\odot$. The triple systems here had circular outer orbits. The remaining parameters have been set to the same values used to produce Fig. 3.

signal are marginal such that its error breaches 50%. The P_2 at which this happens defines the border in Figs. 7 and 8. We see that as the carrier frequency gets larger the outer period can be measured. This is due to this being a redshift

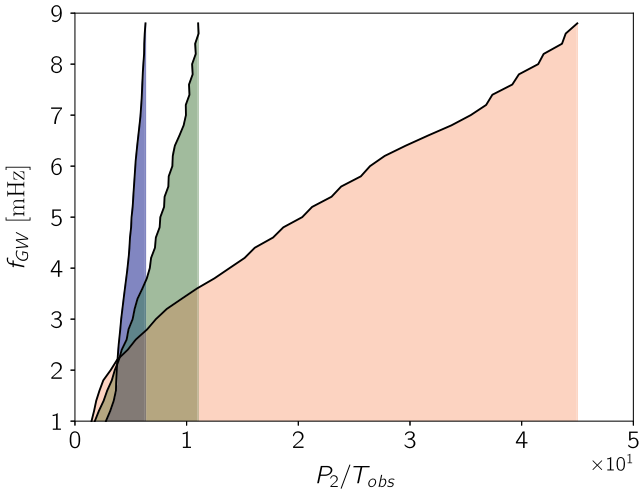

FIG. 8. Just as in the previous figure, the shaded regions denote the triple system which cannot be characterized. Note the orbits period P_2 is given in units of the observation time $T_{\rm obs}$,. These figures are different in that the outer orbits are now eccentric. The red region denotes $e_2 = 0.1$, blue denotes $e_2 = 0.4$, and green denotes $e_2 = 0.9$ These systems had a SNR of 10. We see that more eccentric outer orbits may allow for the characterization of triple systems with much larger outer orbital periods. The mass parameters were chosen to be these same as the previous figure.

phenomenon where the deviations in the frequency observed by LISA are proportional to the frequency itself, coupled with the fact that the error in the frequency is independent (to leading order; see Appendix) of the frequency itself.

Figure 8 reveals the effect that eccentricity of the outer orbit has on the characterization of the triple parameters. Typically, for larger f, increasing the eccentricity allows one to measure orbital periods that are larger than for the circular case. It is important to note that with such large orbits (in fact, any time when $P_2 > T_{\rm obs}$) these results will depend on where we captured the triple in its orbits. For the systems considered here, we chose $\varpi = 0$ and $T_2 = 0$. This Fisher analysis demonstrates that we will be able to characterize the parameters for triple systems of which the orbital period is up to ten times that of the LISA mission lifetime, though the details get slightly modified by the other parameters and SNR.

Let us now address how well the parameters of the triple system can be measured. The period and eccentricity of the outer orbit have the largest effect on the gravitational wave signal and are therefore the most readily measured quantities. It is instructive to consider the strong parallels with the pulsar timing case. The analogy is clear; pulsars in a binary emit pulses at a very regular rate, with mild frequency evolution, and the arrival of these pulses gets modulated by Earth's motion and the presence of a companion. However, for pulsar timing, the source is localized well on the sky, whereas the sky localization is in general poor for galactic binaries detected by LISA [76]. Another parameter that is measured well in pulsar timing is $(m_{\rm b} \sin \iota_2)^3/m_{\rm total}^2$, but it is only with the measurement of a Shapiro time delay for eclipsing binaries which allows the masses and inclination to be untangled. An additional effect, which will be negligible for the triples we are considering, is the variations in the path length of light which allows the longitude of the ascending node Ω_2 to be measured.

Figures 9 and 10 are the results of MCMC of triple systems with a SNR of 50 and a range of outer orbital periods and eccentricities. The injected values are marked by red lines and dots in these figures. As expected, the outer period and eccentricity are measured well for both systems. For both of these systems, the line-of-sight amplitude $\mathcal{A}_2$ is also measured well but, as discussed earlier, on its own not terribly informative, which means that the companion mass cannot be determined. One sees that $\mathcal{A}_2$ and e_2 are correlated, which gets amplified in the more eccentric case. The fact that both of these parameters influence the amplitude of the harmonics induced by the triple is responsible for this correlation. In Fig. 11, marginalized posteriors for the parameters ϖ and T_2 are displayed for the more eccentric system. We see that these quantities are measured well, but they are of little physical interest.

One typically finds that as P_2 increases, such that fewer orbits are captured by LISA, the worse the parameters are

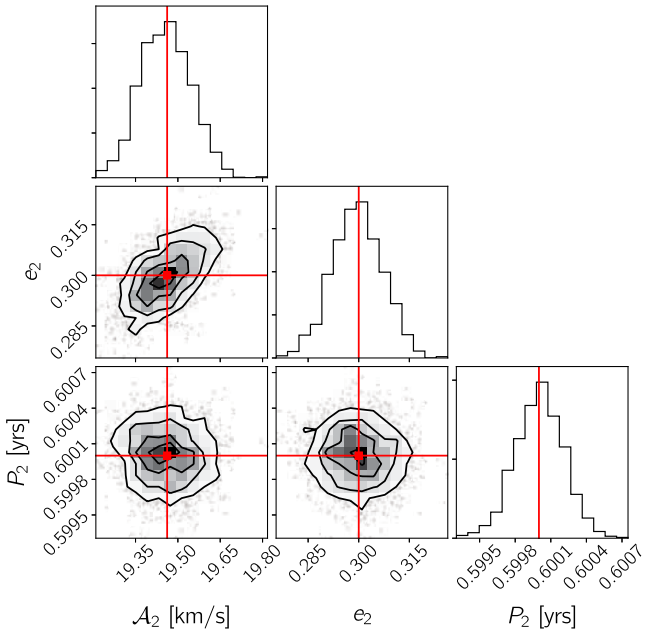

FIG. 9. This is a corner plot of the posteriors for the parameters $\mathcal{A}_2$, e_2, and P_2. The one-dimensional histograms are posteriors marginalized over all other parameters, and the other histograms are joint posteriors between pairs of the aforementioned parameters, marginalized over the rest of the triple system parameters. The line-of-sight velocity amplitude is 19.5 km/ sec, its eccentricity is 0.3, and outer period is 0.6 years. The remaining parameters were chosen to be the same as those chosen in Fig. 3.

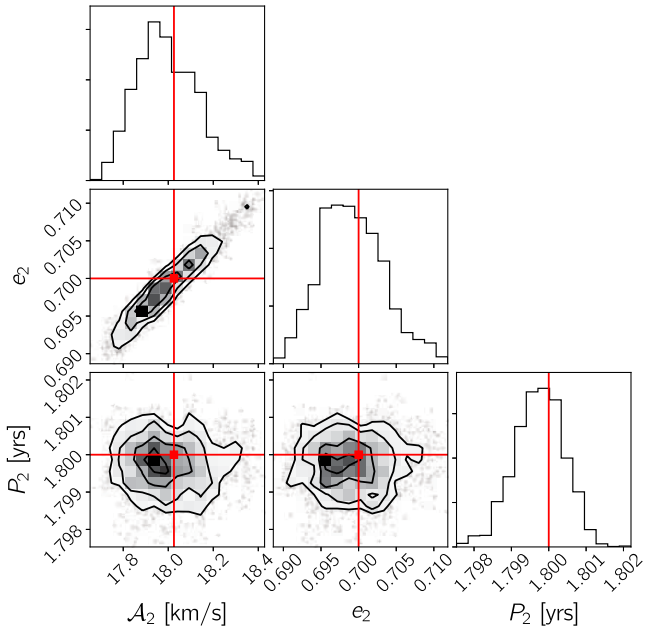

FIG. 10. This corner plot displays some marginalized posteriors for a more eccentric system with a larger outer period. The line-of-sight velocity amplitude is 18.0 km/ sec, its eccentricity is 0.7, and the outer period is 1.8 years. The other parameters were chosen to be the same as the previous corner plot figure.

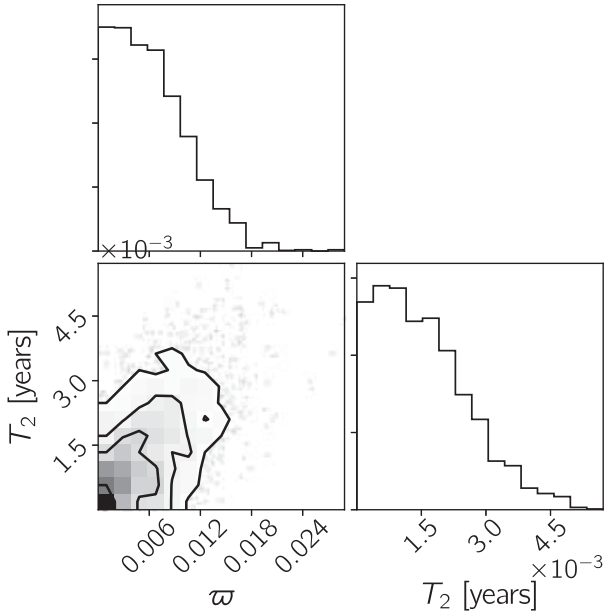

FIG. 11. These are marginalized posteriors for the variables ϖ and T_2 for the system represented by Fig. 9. Both ϖ and T_2 were set to 0 for this system.

characterized. In Fig. 10, the eccentricity has a standard deviation of 0.6% relative to e_2, and the outer period has a standard deviation of 0.037% or 14.6 hours. The tighter system with $P_2 = 0.6$ years had its outer orbital period determine a standard deviation of 4.5 hours. However, this does not seem to hold steadfast for the measurement of eccentricity. The tighter system had a relative standard deviation of 2.5%, i.e., larger than the system with a wider orbit. This exception occurs as the outer orbital period starts to encroach upon the LISA modulation frequency (one year). The distribution of power in the higher modes of the carrier frequency, induced by the triple, get shifted as e_2 changes. These harmonics, when their fundamental frequency $1/P_2$ is comparable to the LISA modulation frequency, begin to interfere strongly, making it harder to accurately extract the eccentricity.

By considering the posteriors in presented in this section, we see that the outer orbital period and outer eccentricity are well-measured parameters.

Lastly, we would like to address the effect of eccentricity in the inner orbit on the characterization of the outer orbital parameters. To do this, we injected a signal with $e_1 = 0$, a SNR of 20, $e_2 = 0.3$, and $P_2 = 0.6$ yr. Again, all other parameters were set to those for Fig. 3. A MCMC was used to calculate the marginalized posterior for the outer orbital parameters denoted by the solid blue line in the upper panels of Fig. 12. Next, a signal where the inner binary was eccentric was simulated; the parameters were set exactly the same as before but with $e_1 = 0.1$ and $\beta_1 = 0$. The resulting marginalized posteriors are displayed by the dashed red line in the upper panels of Fig. 12. As an

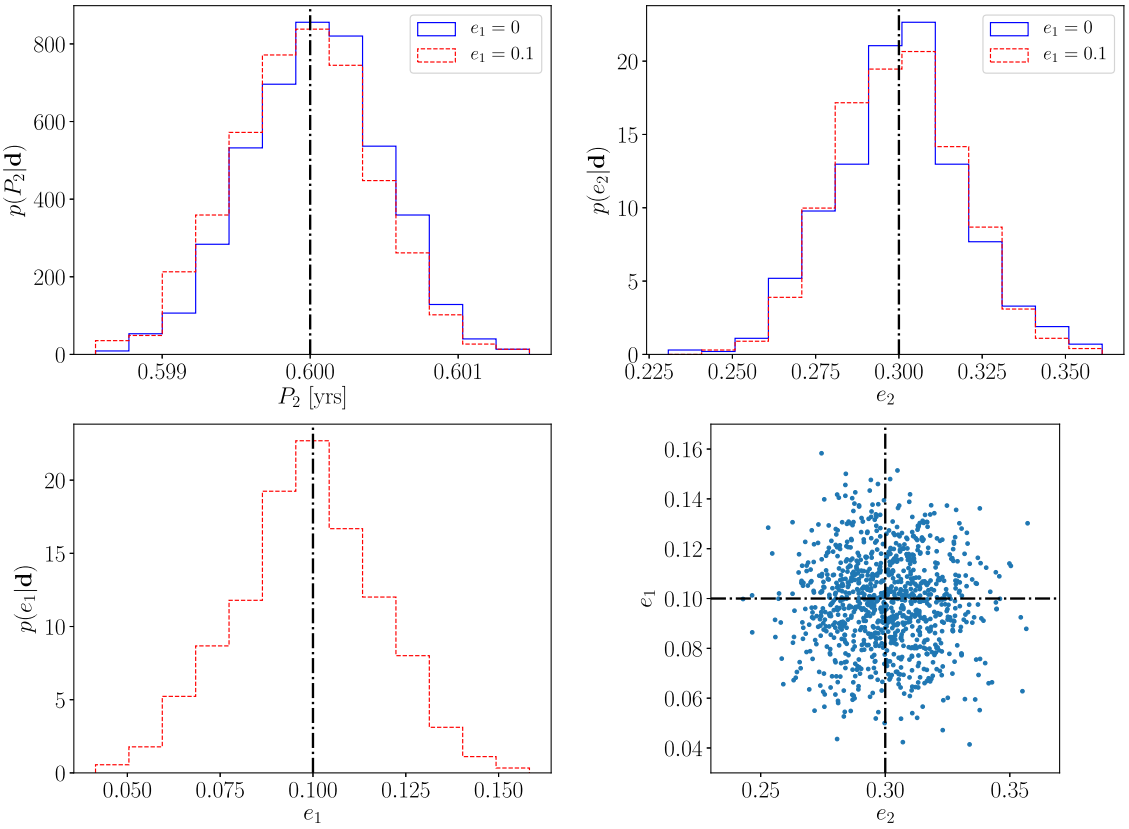

FIG. 12. The solid blue lines denote marginalized posteriors for outer orbital parameters for a circular inner binary injection in the upper panels. The red dashed lines represent the marginalized posteriors for the same parameter for eccentric inner binary injections. The vertical black lines denote the injected parameter values. The marginalized posteriors in the upper panel are statistically equivalent for each parameter. The lower left panel displays the marginalized posterior for the inner eccentricity. The lower right panel is a scatter plot of the e_1 and e_2 samples from the MCMC and shows no correlation.

added bonus, we obtain the marginalized posterior for the inner eccentricity displayed in the lower left panel of the same figure. Since there is zero posterior weight at $e_1 = 0$ this eccentricity is measurable.

Comparing the posteriors for the important and measurable outer binary parameters e_2 and P_2, we see that they are essentially the same distribution. More specifically, the posteriors for the inner eccentric case lie well within the error associated with the posteriors for the inner circular case. Thus, we can conclude that the presence of harmonics in the gravitational waveform due to the existence of eccentricity in the inner binary does not affect the characterization of the outer orbital parameters. The evidence for this is also seen by the lack of any correlation between the outer orbital parameters and e_1. A scatter plot of e_1 and e_2 is displayed in the lower right panel of Fig. 12, and no correlation is evident. This results from the clean separation of harmonics, i.e., the fact that the bandwidth of each harmonic in frequency is much less than their spacing in frequency. Thus, the results we have derived for binaries with circular inner orbits apply unchanged to systems where the inner orbit is eccentric.

VIII. AMBIGUOUS SYSTEMS

Assuming a nominal four year mission lifetime, its been estimated that frequency evolution due to gravitational wave emission or mass transfer will be measurable for roughly 9000 isolated galactic binaries [2]. It is interesting to consider if a regime where the orbital acceleration due to hierarchical companions may be confused with these effects exists. The chance of confusion is greatest when only f and $\dot{f}$ are measurable. In most cases, a measurement of $\ddot{f}$ will break the degeneracy. To determine the risk of confusion, consider Fig. 13, which compares the frequency evolution for an isolated binary and a binary in a hierarchical system. The frequency range over which the effects might be confused is very small since the frequency evolution scales very differently: $\dot{f} \propto f$ from the hierarchical orbit [see Eq. (24)] and $\dot{f} \propto f^{11/3}$ for mass transfer and gravitational wave emission. We see that for an outer period of one year there is no chance of confusion for this system. Even up to outer periods of ten years, the amount of overlap is small. The system with an outer period of 30 years, which is approaching the largest period for which there is a measurable $\dot{f}$, has the greatest potential for

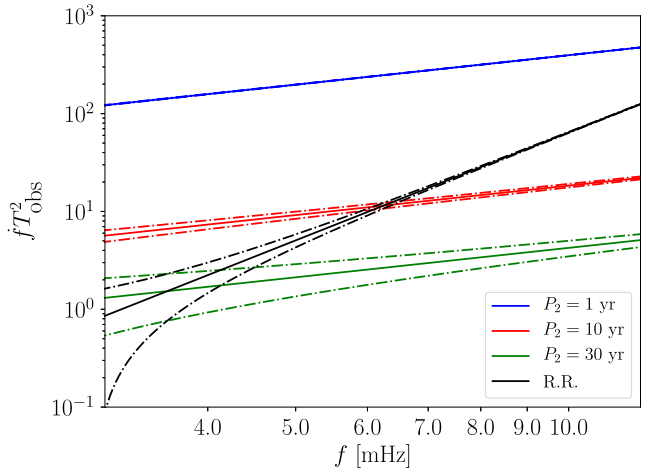

FIG. 13. The solid lines denote the gravitational wave frequency for an isolated binary and for several binaries in hierarchical orbits with outer periods of 1, 10, and 30 years. In each case, the outer orbit is circular, and the SNR of the gravitational wave signal is $\rho = 50$. The dotted lines indicate the Fisher matrix error estimate for the frequency derivatives. Note the difference in power laws for the frequency derivatives and the small region of overlap between the curves. The chirp mass was chosen to be 0.32 $M_\odot$, $m_2 = 2\ M_\odot$, $m_c = 1\ M_\odot$.

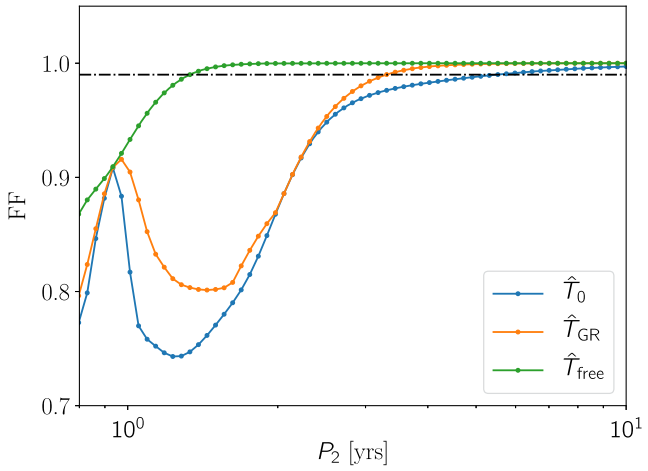

FIG. 14. The blue line represents the fitting factor for a purely monochromatic galactic binary mode $\hat{T}_0$), the orange includes $\dot{f}$ in the frequency evolution ($\hat{T}_{\rm GR}$), and the red includes $\dot{f}$ and $\ddot{f}$ ($\hat{T}_{\rm free}$). These fitting factors are for circular outer orbits. As the outer orbital period increases, the ability of the binary model to match the triple signal is improved. The parameters θ, ϕ, ψ, and ϕ_0 were chosen to be the same as Fig. 3 for the injected triple signal.

confusion. The larger the gravitational wave frequency, the less likely it is that the effects will be confused.

We now directly test how well a binary signal can reproduce a triple signal. To do so, we inject a triple system into the LISA data stream and perform a MCMC with simulated annealing utilizing a galactic binary waveform model. The simulated annealing cools down the MCMC such that the chain settles into the peak of the posterior, thus allowing us to find the best values for the parameters as suggested by the data. The maximum posterior signal allows us to calculate the fitting factor (FF)

$$FF = \max_{\boldsymbol{\lambda}} \frac{(h_{\rm T}|h(\boldsymbol{\lambda}))}{\sqrt{(h_{\rm T}|h_{\rm T})(h(\boldsymbol{\lambda})|h(\boldsymbol{\lambda}))}}, \tag{39}$$

where $\boldsymbol{\lambda}$ are the parameters which maximize the galactic binary model. The fitting factor is a measure of how well the maximum posterior galactic binary waveform $h(\boldsymbol{\lambda}_{\rm max})$ resembles the true triple waveform $h_{\rm T}$, which returns 1 when the signals are equivalent and 0 when they are perfectly orthogonal.

In Fig. 14, we show an example where the observation period was one year and the carrier frequency f was 3 mHz for a circular outer orbit. We are now strictly concerned with how well we can fit a triple signal with an isolated binary model, not with how well parameters can be measured. The relevant masses for the triple were as follows: $m_a = 0.5\ M_\odot$, $\mathcal{M} = 0.32\ M_\odot$, and $m_c = 1.0\ M_\odot$. The parameters T_2 and ω_2 were set to 0. There are three different models under consideration which will be used to fit the injected signal from a triple system. The symbol $\hat{T}$ indicates models that use a Taylor expanded frequency evolution. The $\hat{T}_0$ model assumes the signal is monochromatic, i.e., it is characterized by only f. The $\hat{T}_{\rm GR}$ model utilizes a three-term Taylor expansion (i.e., f, $\dot{f}$, and $\ddot{f}$) in which the coefficients are related by the radiation reaction equations. Lastly, we consider the model $\hat{T}_{\rm free}$ which also utilized a three-term Taylor expansion, but one in which there is no relation between the coefficients.

The $\hat{T}_0$ model is able to fit the signal from the hierarchical system for outer orbital periods that exceed ~4 times the observation period, while the $\hat{T}_{\rm GR}$ model does a little better and is able to fit the signal for outer orbital periods that exceed ~3 times the observation period. The $\hat{T}_{\rm free}$ mode provides a good fit for outer orbital periods that exceed ~1.2 times the observation period. When the outer period is comparable to, or shorter than, the observation time, the Taylor expansion representation of the frequency evolution will begin to fail, and we need to use the full orbital model. Note that in a time-evolving analysis of the LISA data, where the analysis is updated as the data arrives on Earth, the simple Taylor expansion model will initially work well for all systems, but as time goes on, it will begin to break down for systems in hierarchical orbits. Long before that happens, it will be obvious that these systems are part of a hierarchical system as the frequency derivatives will be far in excess of what we expect from mass transfer or gravitational wave emission (or equivalently, the chirp masses needed to explain the frequency evolution in terms of gravitational wave emission will be much larger than is expected for stellar remnants).

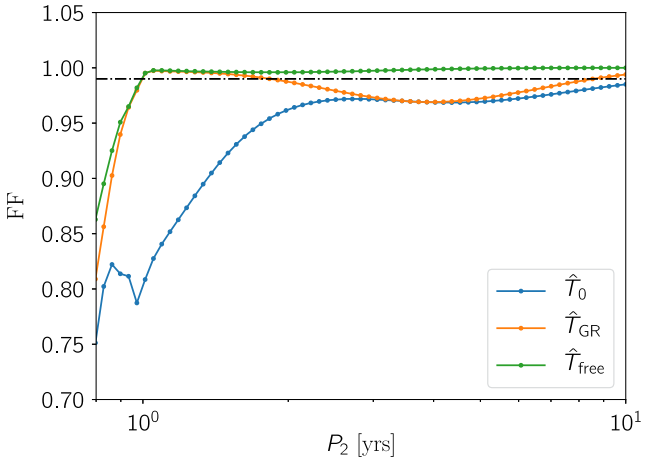

FIG. 15. The fittings factors between an isolated binary model and a highly eccentric triple system are displayed above. These systems have a large eccentricity, $e_2 = 0.7$. Fitting factors are larger compared to the circular outer orbit case in the previous figure.

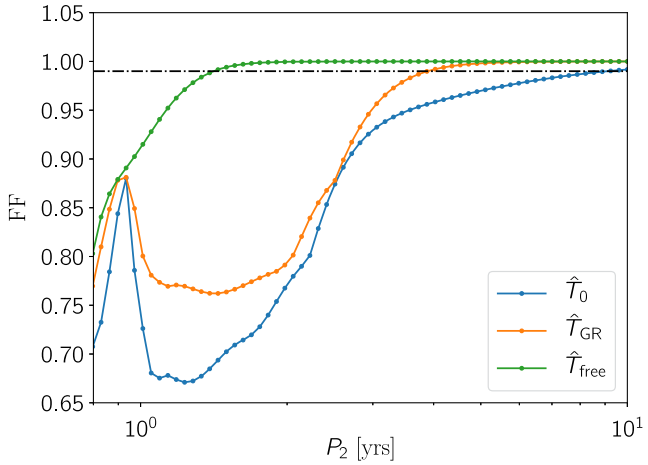

FIG. 16. These triples systems have a circular outer orbit, but the carrier frequency is 5 mHz. This is more challenging for the isolated binary model to replicate the triple data, resulting in worse fitting factors.

The dashed horizontal black line in Fig. 14 denotes a fitting factor of 99%, which is what we expect for a perfectly modeled signal with SNR 20. For a given SNR and model dimension D (for which the galactic binary models we are considering vary from 7 to 9), the presence of noise will cause the fitting factor to deviate from unity even with a perfect model for the signal. The expectation value for the fitting factor in the presence of noise is [77]

$$FF = 1 - \frac{D-1}{2\rho^2}. \tag{40}$$

Above the dashed line, it may not be possible to distinguish the Taylor expanded models from the full hierarchical model, though it will still be possible measure some parameters of the hierarchical orbit past where the dashed black line and fitting factor lines cross. Figure 13 allows one to see what outer periods could reproduce $\dot{f}$'s, which resemble radiation reaction, i.e., when the tracks overlap.

In Fig. 15, the eccentricity of the outer orbit is set to 0.7. We see that the same general description holds. The fitting factors for the various Taylor expansion models decrease as P_2 approaches the LISA orbital timescale. The details of the interference's effects on the fitting factor change, and the fitting factors on the left side of the plot are generally a little higher. This is due to the shift of power to higher modes in the sidebands due to the larger eccentricity such that the most visible fundamental mode has less power. There is again no danger here of mismodeling, as even larger frequency derivatives will be needed to accurately model these signals. Lastly, in Fig. 16, we see how a 5 mHz source compares. We see that again the broad picture is intact, but the outer period at which the Taylor expanded models proves an "acceptable" fitting factor grows, leaving even less room for confusion between the models.

IX. DISCUSSION

Motivated by the possibility that many of the galactic binaries observed by LISA may belong to hierarchical systems, we sought to answer three main questions:

(1) Under what circumstances can we detect the effects on a binary in a triple system?
(2) How well can we characterize the outer orbit of this system?
(3) Where in parameter space might we confuse a triple system with an isolated binary.

The frequency evolution incurred by a center-of-mass acceleration of the inner binary due to the presence of a perturbing companion will be measurable for outer periods as many as ten times larger than the LISA mission lifetime. The outer orbital period and eccentricity will be measurable for systems of which the outer periods are no larger than a few times the LISA mission lifetime. LISA will likely detect many triple systems and characterize their orbits and in doing so provide unique insights into the role that hierarchical companions have on binary evolution.

There will only be a small regime of parameter space in which we would expect to confuse the frequency evolution of an isolated binary with that imparted by a hierarchical companion. Analysis of the LISA data will require a global fit, simultaneously considering all detectable sources to account for covariances between the signals. One might be concerned about how the presence of binaries in hierarchical orbits will complicate the analysis, but it is only a mild complication. The simple Taylor expansion model will pick up the signals accurately at first, and once it becomes clear that the systems are undergoing large accelerations due to a distant companion, the signal model can be switched to the full orbital model.

There are many avenues for future research. For sufficiently tight systems, Lidov-Kozai oscillation or finite size effects may be measurable. Another interesting scenario is that of eclipsing systems. In pulsar timing, an eclipsing system allows one to disentangle the mass and inclination of a binary through the measurement of time delays in the light. For a triple system, the eclipsing companion might induce a measurable Shapiro time-delay-type effect into the gravitational wave, allowing us to learn more about the system.

ACKNOWLEDGMENTS

T. R. and N. J. C. appreciate the support of NASA Grant No. NNX16AB98G. S. T. acknowledges support from the Netherlands Research Council NWO [VENI grant (Grant No. 639.041.645)]. We benefited from useful discussions with Valeria Korol and would like to thank the organizers of the School on Gravitational Waves for Cosmology and Astrophysics held in Benasque where initial ideas for this work were developed.

APPENDIX: BASIC BINARY FISHER ANALYSIS

In this Appendix, we generalize the toy model introduced by Seto [67], which approximates rather well the errors in parameter estimation that one faces with a galactic binary signal in LISA. We model the signal as $h = A\cos(2\pi f_{\rm gw} t + \phi)$, where A is a constant amplitude, ϕ is an arbitrary phase shift, and $f_{gw} = f + \dot{f}t + \frac{1}{2}\ddot{f}t^2$ (note the difference in $\frac{1}{2}$ for the definition between our $\dot{f}$ and Seto's). In this section, we will investigate how the error analysis changes as we include more or fewer parameters in the model.

Under the assumption that the gravitational wave frequency is mildly chirping (such that the Taylor expansion is valid), one may approximate the noise-weighted inner product in the time domain as

$$(g|k) = \frac{2}{S_n(f)}\int_0^T g(t)k(t)dt. \tag{A1}$$

The Fisher matrix, in the approximation in which many cycles are measured, i.e., $fT_{\rm obs} \gg 1$, can be approximated as

$$\Gamma \approx \rho^2 \begin{pmatrix} 1 & 0 & 0 & 0 & 0 \\ 0 & \frac{4}{3}\pi^2T^2 & \pi^2T^3 & \frac{2}{5}\pi^2T^4 & \pi T \\ 0 & \pi^2T^3 & \frac{4}{5}\pi^2T^4 & \frac{1}{3}\pi^2T^5 & \frac{2}{3}\pi T^2 \\ 0 & \frac{2}{5}\pi^2T^4 & \frac{1}{3}\pi^2T^5 & \frac{1}{7}\pi^2T^6 & \frac{1}{4}\pi T^3 \\ 0 & \pi T & \frac{2}{3}\pi T^2 & \frac{1}{4}\pi T^3 & 1 \end{pmatrix}, \tag{A2}$$

where the matrix is ordered as $\log A$, f, $\dot{f}$, $\ddot{f}$, ϕ. Upon inversion, we may obtain estimates of the errors in the parameters of interest by inverting the full Fisher matrix (or in versions where the $\ddot{f}$ and/or $\dot{f}$ dimensions are dropped). When only a monochromatic signal is used, the rms errors are

$$\Delta f T_{\rm obs} = \frac{\sqrt{3}}{\pi}\rho^{-1} \approx 0.06\left(\frac{10}{\rho}\right) \tag{A3}$$

$$\Delta\phi = 2\rho^{-1} \approx 0.20\left(\frac{10}{\rho}\right). \tag{A4}$$

Including $\dot{f}$ inflates the errors to the following:

$$\Delta f T_{\rm obs} = \frac{4\sqrt{3}}{\pi}\rho^{-1} \approx 0.22\left(\frac{10}{\rho}\right) \tag{A5}$$

$$\Delta \dot{f} T^2_{\rm obs} = \frac{3\sqrt{5}}{\pi}\rho^{-1} \approx 0.21\left(\frac{10}{\rho}\right) \tag{A6}$$

$$\Delta\phi = 3\rho^{-1} \approx 0.30\left(\frac{10}{\rho}\right). \tag{A7}$$

Lastly, if one also includes the $\ddot{f}$ term,

$$\Delta f T_{\rm obs} = \frac{10\sqrt{3}}{\pi}\rho^{-1} \approx 0.55\left(\frac{10}{\rho}\right) \tag{A8}$$

$$\Delta \dot{f} T^2_{\rm obs} = \frac{18\sqrt{5}}{\pi}\rho^{-1} \approx 1.28\left(\frac{10}{\rho}\right) \tag{A9}$$

$$\Delta \ddot{f} T^3_{\rm obs} = \frac{20\sqrt{7}}{\pi}\rho^{-1} \approx 1.68\left(\frac{10}{\rho}\right) \tag{A10}$$

$$\Delta\phi = 4\rho^{-1} \approx 0.40\left(\frac{10}{\rho}\right). \tag{A11}$$

Now, we will consider a numerically calculated Fisher matrix for a galactic binary seen by LISA, which includes only f and $\dot{f}$ in its frequency evolution. The following matrix is ordered as f, $\cos\theta$, ϕ, $\log A$, $\cos\iota_1$, ψ, ϕ_0, and $\dot{f}$:

$$\Gamma = \begin{pmatrix} 5.05\times10^{3} & 2.77\times10^{2} & -1.77\times10^{2} & 9.85\times10^{-4} & 2.08 & 2.49\times10^{3} & 1.24\times10^{3} & 1.82\times10^{3} \\ 2.77\times10^{2} & 5.25\times10^{2} & -2.01\times10^{2} & -3.47 & -3.56 & 2.09\times10^{1} & 1.04\times10^{1} & 1.26\times10^{2} \\ -1.77\times10^{2} & -2.01\times10^{2} & 3.15\times10^{4} & 5.87\times10^{-1} & 1.37\times10^{1} & -5.87\times10^{1} & -2.88\times10^{1} & 5.26\times10^{2} \\ 9.85\times10^{-4} & -3.47 & 5.87\times10^{-1} & 4.00\times10^{2} & 4.13\times10^{2} & -6.67\times10^{-1} & 5.52\times10^{-9} & 1.32\times10^{-3} \\ 2.08 & -3.56 & 1.37\times10^{1} & 4.13\times10^{2} & 4.27\times10^{2} & 1.09 & 5.81e-01 & 1.04 \\ 2.49\times10^{3} & 2.09\times10^{1} & -5.87\times10^{1} & -6.67\times10^{-2} & 1.09 & 1.60\times10^{3} & 8.00\times10^{2} & 8.04\times10^{2} \\ 1.24\times10^{3} & 1.04\times10^{1} & -2.88\times10^{1} & 5.52\times10^{-9} & 5.81\times10^{-1} & 8.00\times10^{2} & 4.00\times10^{2} & 4.02\times10^{2} \\ 1.82\times10^{3} & 1.26\times10^{2} & 5.26\times10^{2} & 1.32\times10^{-3} & 1.04 & 8.04\times10^{2} & 4.02\times10^{2} & 6.95\times10^{2} \end{pmatrix}. \tag{A12}$$

This system had a carrier frequency of 5 mHz, a chirp mass of 0.32 $M_\odot$, and a SNR of 20. The Fisher matrix is inverted, providing an estimate of the covariance matrix. The error estimates from this covariance matrix are:

$$\Delta f T_{\rm obs} = 0.31, \tag{A13}$$

$$\Delta \dot{f} T_{\rm obs}^2 = 0.61. \tag{A14}$$

These errors are rather robust to choices in the parameters of the model. Comparing these results to the toy model considered above, we see that the error in f is roughly three times larger when using the full galactic binary model and about six times larger for $\dot{f}$. This results from the very strong covariance between ϕ_0 and ψ tied with the covariance of both of these parameters with f and $\dot{f}$. If one considers galactic binaries modeled with $\ddot{f}$ as well, one finds that the error in $\ddot{f}$ is about four times as great as the toy model estimate. These extra inflations are included in the analysis throughout the body of this paper, in which we consider how tight the outer orbit must be for certain features to be measurable.

[1] H. Audley *et al.*, arXiv:1702.00786.
[2] N. Cornish and T. Robson, J. Phys. Conf. Ser. **840**, 012024 (2017).
[3] D. Raghavan, H. A. McAlister, T. J. Henry, D. W. Latham, G. W. Marcy, B. D. Mason, D. R. Gies, R. J. White, and T. A. ten Brummelaar, Astrophys. J. Suppl. Ser. **190**, 1 (2010).
[4] A. Tokovinin, Astron. J. **147**, 87 (2014).
[5] K. Fuhrmann, R. Chini, L. Kaderhandt, and Z. Chen, Astrophys. J. **836**, 139 (2017).
[6] A. Tokovinin, S. Thomas, M. Sterzik, and S. Udry, Astron. Astrophys. **450**, 681 (2006).
[7] T. Pribulla and S. M. Rucinski, Astron. J. **131**, 2986 (2006).
[8] M. L. Lidov, Planet. Space Sci. **9**, 719 (1962).
[9] Y. Kozai, Astron. J. **67**, 591 (1962).
[10] S. Naoz, Annu. Rev. Astron. Astrophys. **54**, 441 (2016).
[11] T. A. Thompson, Astrophys. J. **741**, 82 (2011).
[12] X. Fang, T. A. Thompson, and C. M. Hirata, Mon. Not. R. Astron. Soc. **476**, 4234 (2018).
[13] S. Toonen, H. B. Perets, and A. S. Hamers, Astron. Astrophys. **610**, A22 (2018).
[14] D. Fabrycky and S. Tremaine, Astrophys. J. **669**, 1298 (2007).
[15] S. Naoz and D. C. Fabrycky, Astrophys. J. **793**, 137 (2014).
[16] K. Silsbee and S. Tremaine, Astrophys. J. **836**, 39 (2017).
[17] F. Antonini, S. Toonen, and A. S. Hamers, Astrophys. J. **841**, 77 (2017).
[18] N. Yunes, M. C. Miller, and J. Thornburg, Phys. Rev. D **83**, 044030 (2011).
[19] Y. Meiron, B. Kocsis, and A. Loeb, Astrophys. J. **834**, 200 (2017).
[20] C. Bonvin, C. Caprini, R. Sturani, and N. Tamanini, Phys. Rev. D **95**, 044029 (2017).
[21] K. Inayoshi, N. Tamanini, C. Caprini, and Z. Haiman, Phys. Rev. D **96**, 063014 (2017).
[22] L. Randall and Z.-Z. Xianyu, arXiv:1805.05335.
[23] R. T. Edwards, G. B. Hobbs, and R. N. Manchester, Mon. Not. R. Astron. Soc. **372**, 1549 (2006).
[24] A. Tokovinin, Astron. J. **147**, 87 (2014).
[25] H. Sana *et al.*, Astrophys. J. Suppl. Ser. **215**, 15 (2014).
[26] N. R. Evans, K. G. Carpenter, R. Robinson, F. Kienzle, and A. E. Dekas, Astron. J. **130**, 789 (2005).
[27] A. Tokovinin, Astron. J. **147**, 86 (2014).
[28] Toonen*et al.* (to be published).
[29] T. A. Thompson, Astrophys. J. **741**, 82 (2011).
[30] H. B. Perets and K. M. Kratter, Astrophys. J. **760**, 99 (2012).
[31] A. S. Hamers, O. R. Pols, J. S. W. Claeys, and G. Nelemans, Mon. Not. R. Astron. Soc. **430**, 2262 (2013).

[32] S. Toonen, A. Hamers, and S. P. Zwart, Comput. Astrophys. Cosmol. **3**, 6 (2016).
[33] S. Toonen, H. B. Perets, and A. S. Hamers, Astron. Astrophys. **610**, A22 (2018).
[34] F. Antonini and H. B. Perets, Astrophys. J. **757**, 27 (2012).
[35] S. Prodan, F. Antonini, and H. B. Perets, Astrophys. J. **799**, 118 (2015).
[36] A. P. Stephan, S. Naoz, A. M. Ghez, G. Witzel, B. N. Sitarski, T. Do, and B. Kocsis, Mon. Not. R. Astron. Soc. **460**, 3494 (2016).
[37] J. H. VanLandingham, M. C. Miller, D. P. Hamilton, and D. C. Richardson, Astrophys. J. **828**, 77 (2016).
[38] B.-M. Hoang, S. Naoz, B. Kocsis, F. A. Rasio, and F. Dosopoulou, Astrophys. J. **856**, 140 (2018).
[39] P. P. Eggleton and F. Verbunt, Mon. Not. R. Astron. Soc. **220**, 13P (1986).
[40] N. Ivanova, S. Chaichenets, J. Fregeau, C. O. Heinke, J. C. Lombardi, Jr., and T. E. Woods, Astrophys. J. **717**, 948 (2010).
[41] S. Naoz, T. Fragos, A. Geller, A. P. Stephan, and F. A. Rasio, Astrophys. J. **822**, L24 (2016).
[42] H. B. Perets and D. C. Fabrycky, Astrophys. J. **697**, 1048 (2009).
[43] L. G. Kiseleva, P. P. Eggleton, and S. Mikkola, Mon. Not. R. Astron. Soc. **300**, 292 (1998).
[44] T. Mazeh and J. Shaham, Astron. Astrophys. **77**, 145 (1979).
[45] A. C. M. Correia, J. Laskar, F. Farago, and G. Boué, Celestial Mech. Dyn. Astron. **111**, 105 (2011).
[46] C. Petrovich, Astrophys. J. **799**, 27 (2015).
[47] Y. Wu and N. Murray, Astrophys. J. **589**, 605 (2003).
[48] S. Naoz, W. M. Farr, Y. Lithwick, F. A. Rasio, and J. Teyssandier, Nature (London) **473**, 187 (2011).
[49] S. Naoz, W. M. Farr, and F. A. Rasio, Astrophys. J. **754**, L36 (2012).
[50] R. I. Dawson and E. Chiang, Science **346**, 212 (2014).
[51] B. Katz and S. Dong, arXiv:1211.4584.
[52] S. Toonen, M. Hollands, B. T. Gänsicke, and T. Boekholt, Astron. Astrophys. **602**, A16 (2017).
[53] K. Gültekin, M. C. Miller, and D. P. Hamilton, Astrophys. J. **640**, 156 (2006).
[54] N. Seto, Phys. Rev. Lett. **111**, 061106 (2013).
[55] L. Randall and Z.-Z. Xianyu, arXiv:1802.05718.
[56] Y. Y. Klein and B. Katz, Mon. Not. R. Astron. Soc. **465**, L44 (2017).
[57] M. A. Hollands, P. E. Tremblay, B. T. Gaensicke, N. P. Gentile-Fusillo, and S. Toonen, Mon. Not. R. Astron. Soc. **480**, 3942 (2018).
[58] S. M. Ransom *et al.*, Nature (London) **505**, 520 (2014).
[59] T. M. Tauris and E. P. J. van den Heuvel, Astrophys. J. **781**, L13 (2014).
[60] E. Sabach and N. Soker, Mon. Not. R. Astron. Soc. **450**, 1716 (2015).
[61] E. B. Ford, B. Kozinsky, and F. A. Rasio, Astrophys. J. **535**, 385 (2000).
[62] R. S. Harrington, Astron. J. **73**, 190 (1968).
[63] C. M. Will, Phys. Rev. D **96**, 023017 (2017).
[64] Y. Kozai, Astron. J. **67**, 591 (1962).
[65] M. L. Lidov, Planet. Space Sci. **9**, 719 (1962).
[66] S. Naoz and D. C. Fabrycky, Astrophys. J. **793**, 137 (2014).
[67] N. Seto, Mon. Not. R. Astron. Soc. **333**, 469 (2002).
[68] T. R. Marsh, G. Nelemans, and D. Steeghs, Mon. Not. R. Astron. Soc. **350**, 113 (2004).
[69] N. J. Cornish and T. B. Littenberg, Phys. Rev. D **76**, 083006 (2007).
[70] J. W. Armstrong, F. B. Estabrook, and M. Tinto, Astrophys. J. **527**, 814 (1999).
[71] T. Robson and N. Cornish, Classical Quantum Gravity **34**, 244002 (2017).
[72] N. Cornish and T. Robson, arXiv:1803.01944.
[73] B. Moore, T. Robson, N. Loutrel, and N. Yunes, arXiv:1807.07163.
[74] N. J. Cornish and J. Crowder, Phys. Rev. D **72**, 043005 (2005).
[75] J. S. Key and N. J. Cornish, Phys. Rev. D **83**, 083001 (2011).
[76] C. Cutler, Phys. Rev. D **57**, 7089 (1998).
[77] K. Chatziioannou, A. Klein, N. Cornish, and N. Yunes, Phys. Rev. Lett. **118**, 051101 (2017).